

## Article

# Mathematical Modeling for the Process of Smelting Reduction Ironmaking Integrated with Hydrogen-Rich Coal Gasification

Yingxia Qu <sup>1,2</sup>, Shihao Song <sup>2</sup>, Zongshu Zou <sup>1,2</sup> and Lei Shao <sup>1,2,\*</sup>

<sup>1</sup> Key Laboratory for Ecological Metallurgy of Multimetallic Mineral (Ministry of Education), Northeastern University, Shenyang 110819, China; quyx@smm.neu.edu.cn (Y.Q.); zouzs@mail.neu.edu.cn (Z.Z.)

<sup>2</sup> School of Metallurgy, Northeastern University, Shenyang 110819, China; 2171667@stu.neu.edu.cn

\* Correspondence: shaolei@smm.neu.edu.cn; Tel.: +86-024-83672053

**Abstract:** To reduce pollution and improve the efficiency of coal resource utilization, this study proposed an integrated process for smelting reduction ironmaking and coal gasification. A multi-zone constrained mathematical model, based on heat and mass balance calculations, was developed to predict the energy and material flows required to produce 1 ton of hot metal. Two scenarios were examined: one using pure O<sub>2</sub> as the gasification agent (referred to as the non-hydrogen-rich process) and the other using a combination of pure O<sub>2</sub> and pure steam (referred to as the hydrogen-rich process). In the non-hydrogen rich process, as the PCR (Post Combustion Ratio) varies from 0% to 8%, the total coal consumption, O<sub>2</sub> consumption, and volume of exported gas decrease by 57%, 57% and 53%, respectively. In the hydrogen-rich process, as the H<sub>2</sub> content increases from 30% to 50%, the exported gas volume increases by 38%. The upper limit of H<sub>2</sub> content in the SRV (Smelting Reduction Vessel) off-gas is mainly determined by the PCR, which decreases from 52.7% to 45.2% as the PCR varies from 0% to 8%. The findings of this work can serve as a theoretical basis for further investigation of the new process.

**Keywords:** mathematical modelling; ironmaking; coal gasification; hydrogen-rich process



**Citation:** Qu, Y.; Song, S.; Zou, Z.; Shao, L. Mathematical Modeling for the Process of Smelting Reduction Ironmaking Integrated with Hydrogen-Rich Coal Gasification. *Processes* **2024**, *12*, 370. <https://doi.org/10.3390/pr12020370>

Academic Editor: Adam Smoliński

Received: 22 December 2023

Revised: 6 February 2024

Accepted: 8 February 2024

Published: 10 February 2024



**Copyright:** © 2024 by the authors. Licensee MDPI, Basel, Switzerland. This article is an open access article distributed under the terms and conditions of the Creative Commons Attribution (CC BY) license (<https://creativecommons.org/licenses/by/4.0/>).

## 1. Introduction

Coal, as one of the most crucial resources in the world, is extensively used in industries such as iron and steel, coal chemical, and power generation. However, with the increasing prominence of environmental issues, the use of coal is facing a series of challenges [1,2]. Long-term production practices in the coal chemical industries have demonstrated that coal gasification is pivotal for improving economic efficiency and reducing environmental pollution. On the other hand, most current coal gasification processes yield syngas with relatively low effective gas content (Hydrogen, H<sub>2</sub> and Carbon monoxide, CO), especially the H<sub>2</sub> content [3–6]. For example, Lurgi and British Gas Lurgi are two representative commercialized coal gasification technologies. Compared to Lurgi, British Gas Lurgi technology is capable of operating under a higher temperature, thus resulting in a better gasification efficiency. The effective gas composition of CO and H<sub>2</sub> in the syngas produced by Lurgi technology ranges from 54% to 68%, and the effective gas composition of CO and H<sub>2</sub> obtained from British Gas Lurgi technology is lower than 85% [7–9].

To achieve a highly economical, environmentally friendly, and high-quality syngas production technology, extensive research has been conducted on a new method that utilizes high temperature molten metal media. In 1978, Sumitomo Metals Corporation from Japan proposed a process that combines steelmaking with coal gasification, known as the “CGS process” [10]. This process involves simultaneously injecting pulverized coal, O<sub>2</sub> (Oxygen), and steam into the molten iron in the converter furnace through lances. The molten iron temperature ranges between 1400 °C and 1600 °C. Small-scale studies have revealed that approximately 90% of the gas produced is CO and H<sub>2</sub>, and the desulfurization effect

by the molten slag is higher than 95%, resulting in very low amounts of H<sub>2</sub>S (Hydrogen sulfide), COS (Carbon oxysulfide), and other harmful substances in the gas [11]. In the 1980s, a similar pilot steel plant was built for the integration of steelmaking and coal gasification in Luleå, northeast Sweden. The process is named as “MIP” (Molten-Iron-Pure-Gas) [12]. The pulverized coal and O<sub>2</sub> are injected into the molten iron from the bottom of the furnace. It has been found that this process could also produce high-quality gas, and most of the sulfur in the raw materials enters the slag phase, leading to a significant reduction in sulfur emissions. Additionally, compared to the top blowing method in the CGS process, the MIP process forms a foamy slag layer, increasing the residence time of reactants in the slag and reducing the generation of dust. In 2007, a two-step process for producing hydrogen-rich syngas was developed by Diversified Energy Corporation and Alchemix Corporation, known as HydroMax [13,14]. The main reactor was designed with reference to HIs melt (High intensity smelting) which is a smelting reduction ironmaking process. In this process, a molten metal bath of iron-tin alloy at 1250 °C is injected with superheated steam and coal separately during different periods of time. The iron in the bath is first oxidized by steam to form iron oxide and release H<sub>2</sub>-rich syngas, and then the iron oxide is reduced by carbon to obtain metallic iron and CO-rich syngas. The results show that HydroMax can effectively produce H<sub>2</sub>-rich syngas with very few impurities due to their capture in the molten metal bath. Although these technologies have not yet achieved large-scale production, the research results have already indicated that coal gasification in high temperature molten metal media can enhance the quality of syngas and reduce environmental pollution.

In recent years, several iron bath smelting reduction technologies, such as HIs melt, HIsarna, and flash ironmaking technology, have been successfully tested and are becoming increasingly mature [15–17]. These processes involve a final reduction step in a high-temperature Smelting Reduction Vessel (SRV) containing molten iron and slag. HIs melt has been in development for over 40 years and successfully commercialized. Based on the successful experience of the HIs melt process, Hisarna has been proposed by combining the cyclone furnace of CCF (Cyclone Converter Furnace) technology and the SRV of HIs melt technology [18–20]. The flash ironmaking technology utilizes a Flash Reduction Shaft (FRS) and a SRV, but unlike HIs melt and Hisarna, it uses H<sub>2</sub> or natural gas instead of coal as the reducing agent and fuel [21–23]. A portion of the heat required in the reactor is provided by the combustion of H<sub>2</sub> or natural gas with O<sub>2</sub>, but external heating may be necessary since the Post Combustion Ratio (PCR) of gas in the SRV should not be very high. In the FRS, iron oxide fines can be pre-reduced to a high reduction degree (>90%) within a few seconds, and then collected in the molten bath for steelmaking [21,24].

Based on the extensive research findings on iron bath smelting reduction processes [25,26] and the coal gasification in molten metal media, this study proposes a new integrated technology of smelting reduction ironmaking and coal gasification as shown in Figure 1a. The process consists of three main sections: an FRS for pre-reduction of iron ore fines, a SRV for final reduction, and an uptake shaft for gas reforming. The energy required by the FRS is provided by the sensible heat of reformed gas and the heat generated by the combustion of reformed gas with pure O<sub>2</sub>. The pre-reduced iron ore fines (with a pre-reduction degree) then fall into the bath of the SRV, which has a thick slag layer situated above the hot metal. This thick slag layer provides the necessary space for iron oxide reduction and coal gasification [27]. In addition, it can filter out the pollutants from the syngas [12,14]. The SRV is equipped with three-layer lances to improve the energy utilization and facilitate flexible control of the production conditions inside the reactor. The two lower layers of lances inject pulverized coal and pure O<sub>2</sub> into the thick slag layer to provide a reducing and gasification agent, while the top layer of lances inject O<sub>2</sub> into the free space to provide energy through combustion reactions if necessary. To ensure production of high-quality syngas, the PCR of the SRV off-gas is controlled below 10%. The high-temperature SRV off-gas and FRS off-gas then pass through the uptake shaft, into which pulverized coal is injected for gas reforming. A small portion of the reformed gas

(the off-gas of the uptake shaft) is recycled into the FRS as a reducing agent and fuel, while the remaining gas, referred to as exported gas in Figure 1a, can be used by other reactors in the steel plant or used as a raw material in the chemical industry [28].

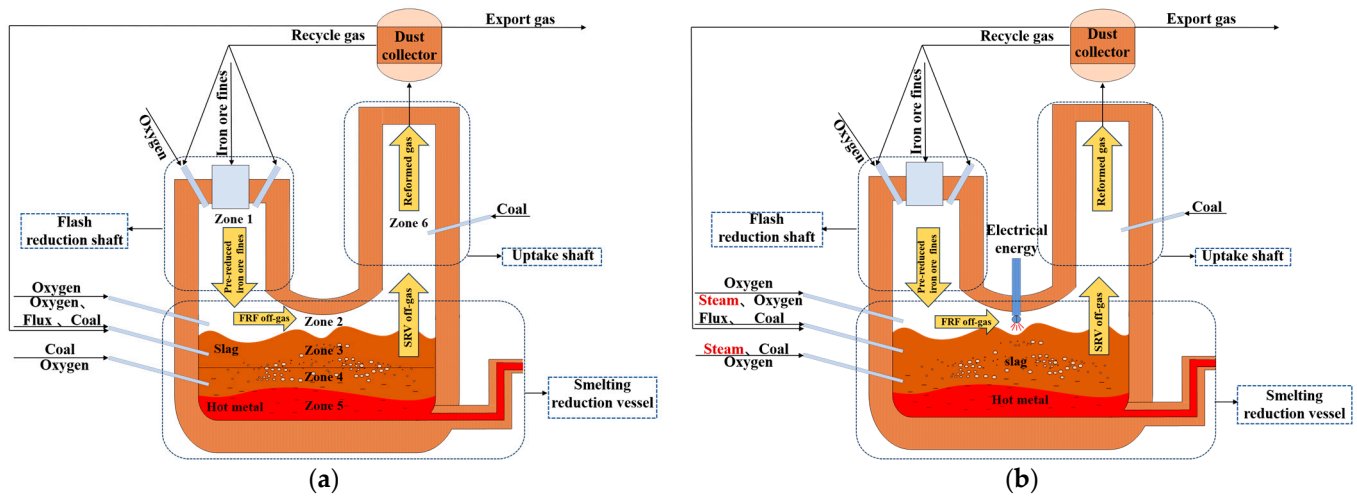


**Figure 1.** Schematic diagram of integrated technology of smelting reduction ironmaking and coal gasification: (a) oxygen as coal gasification agent; (b) oxygen and steam as coal gasification agent.

Under this situation,  $O_2$  is utilized as the only one gasification agent and  $H_2$  is primarily derived from the volatile matter in the coal and the moisture in the materials. As a result, the  $H_2$  content in the produced syngas is relatively low, which restricts the potential applications of the syngas. To address this issue, an alternative process of injecting pure steam instead of a portion of  $O_2$  into the thick slag bath is taken into account, as shown in Figure 1b. Steam can be produced by steam boilers. In situations where there is insufficient heat in the SRV, electric energy can be utilized for heating. This study refers to the two processes (Figure 1a,b) as the non-hydrogen rich process and the hydrogen-rich process, respectively.

For new or improved technologies, the heat and mass balance calculation, also known as a static model, is useful for obtaining detailed information about material and energy flows and for evaluating the process feasibility. This kind of model is formulated based on the mass and heat balance in conjunction with principles of equilibrium thermodynamics [29]. For example, Wang et al. [30] established a static model to assess the mass and heat balance of the electric arc furnace steelmaking process with the introduction of  $CO_2$  as a diluting gas. Similarly, Bhaskar et al. [31] developed a heat and mass balance model to explore the feasibility of using a hydrogen direct reduction of iron ore coupled with an electric arc furnace for steel production. They calculated the specific energy consumption and  $CO_2$  emissions for the production of 1 ton of liquid steel. In another study, Jampani et al. [32] examined the potential for increased use of natural gas in a blast furnace using a static model and determined the optimal operating window for tuyere and shaft injection of natural gas. Kou et al. [33] proposed a method for adjusting the freeboard temperature of the COREX (Coal reduction extreme) melter gasifier by injecting coke oven gas from the dome, and the effect of this injection was predicted using a static model. When the first COREX-3000 plant was built in China, the author of this paper also developed a static model for the COREX process. However, most of the previous models only considered the mass and heat balances of the furnace as a whole. The integrated technology in this study can achieve a coupling of manufacturing of iron and syngas, which would make most sense in the clean and efficient utilization of coal resources. In order to gain more insight into the furnace, a multi-zone constrained mathematical model was developed to predict material and energy flows of the processes.

## 2. Model Description

The present model assumes that the process operates at a steady state, and the mass balance calculation is based on producing 1 ton of hot metal. The furnace is notionally divided into six zones: the FRS, the free space of SRV, the upper slag zone of SRV, the lower slag zone of SRV, the hot metal zone, and the uptake shaft (as shown in Figure 1). The FRS is the main reactor for pre-reduction and melting of iron ore fines. The PCR of gas can be adjusted in the free space of SRV. The upper slag and lower slag zones are essential for melting solid materials and for the final reduction of iron oxides. The generated hot metal is collected in the bottom zone, and it is assumed that no reaction takes place in this zone. The main constraints for each zone are given in Figure 2. The average reaction temperature in the FRS, the temperature of the slag, and the temperature and composition of the hot metal are determined based on production data from the flash ironmaking technology and HIs melt processes [26,34,35]. The PCR of gas in the upper and lower slag zones are limited to 0% to prevent secondary oxidation of metallic iron. The reaction between C and CO<sub>2</sub> does not proceed significantly below 900 °C [36]. Therefore, the reformed gas temperature at the outlet of the uptake shaft is required to be higher than this value.

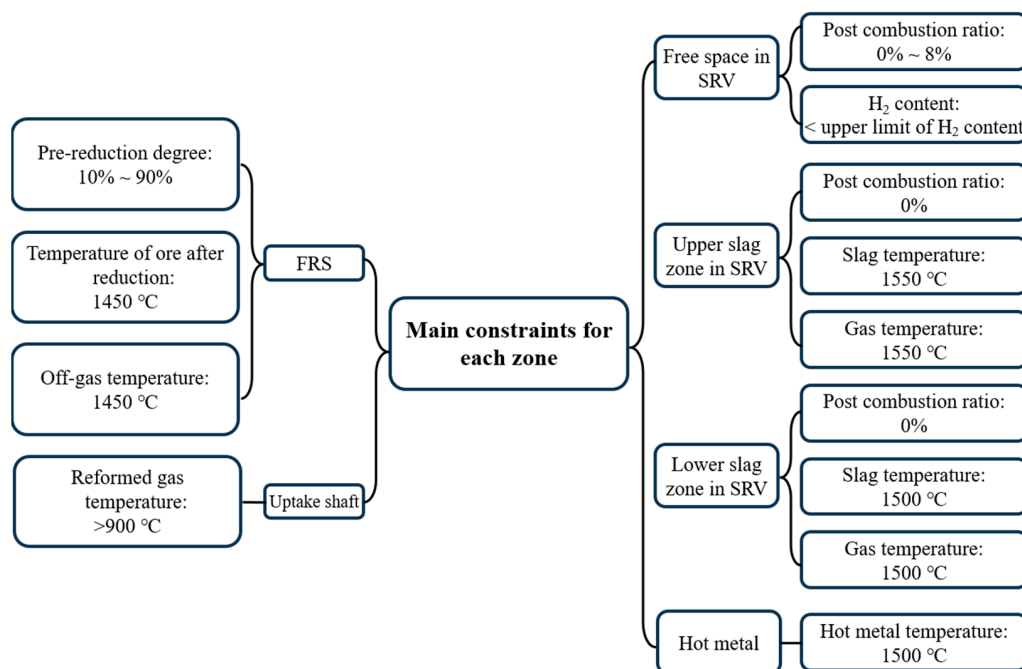
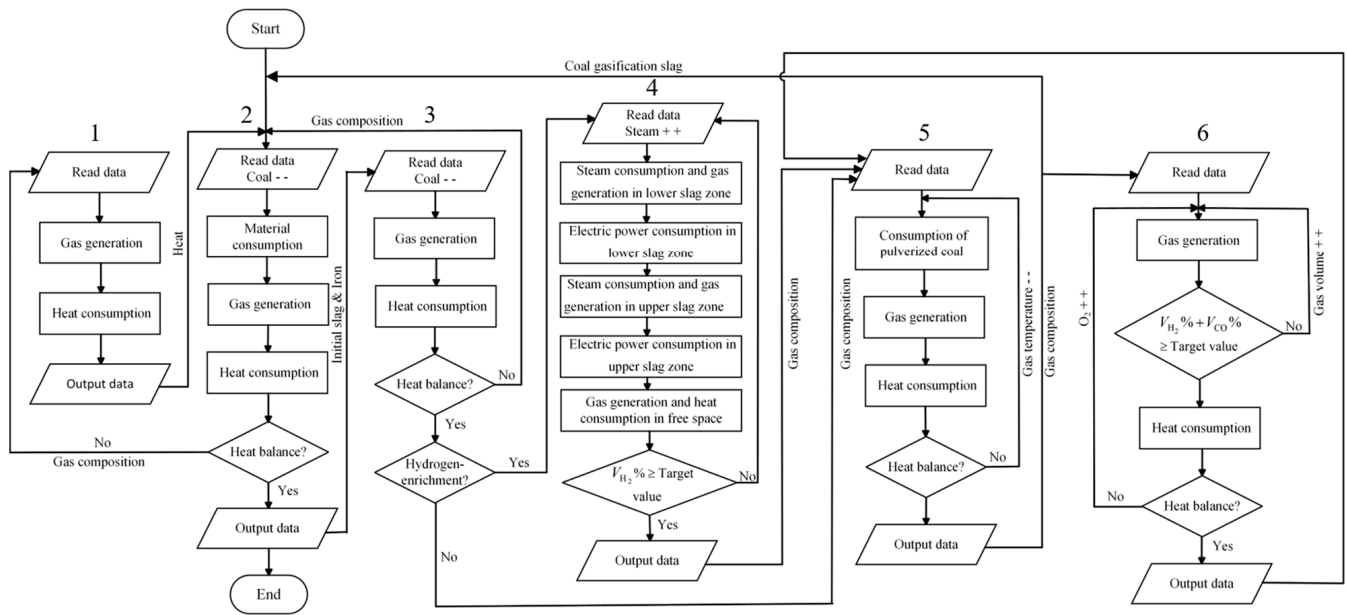


Figure 2. Main constraints for six zones in the reactor.

Since the composition and temperature of hot metal are known conditions for the model, the calculation for the hot metal zone is straightforward. This work uses five modules (No. 1, 2, 3, 5, and 6) to calculate the remaining five zones, and the five modules are interconnected as a complex mathematical model that is solved using an iterative algorithm. The concept of the model is illustrated as a flow chart in Figure 3. The heat balances in the three zones of the SRV and the uptake shaft are closed by the coal consumptions, and the heat balance in the shaft furnace is closed by reducing gas consumption or O<sub>2</sub> consumption. In the case of producing hydrogen-rich gas, the module 4 is activated. The amount of steam replacing the O<sub>2</sub> injection is determined by the target H<sub>2</sub> content in the SRV off-gas. In order to compare the hydrogen-rich and non-hydrogen-rich processes, the model ensures that the coal consumption is the same for both processes. Additionally, the upper limit of H<sub>2</sub> content in the off-gas of the SRV can be achieved when all the O<sub>2</sub> is replaced by steam. The calculation methods for the main parameters of the process are explained in the following context.



1. Calculation for free space of SRV 2. Calculation for upper slag zone 3. Calculation for lower slag zone  
4. Calculation for steam injection 5. Calculation for uptake shaft 6. Calculation for FRS

**Figure 3.** Flow chart of the present multi-zone constrained mathematical model.

### 2.1. Main Calculation Methods for SRV

The heat and mass balance calculation for the three zones of SRV is processed using the three coupled mathematical modules 1–3. The consumption of iron ore and fluxes, as well as the slag rate (mass of slag for producing 1 ton of hot metal), are calculated by module 2 through solving a set of equations. The equations include iron element balance, binary basicity  $R_2$ , quaternary basicity  $R_4$ , and slag mass (Equations (1)–(4)). This also allows for achieving the composition of slag.

- Fe balance:

$$\sum_i m_i \times w[\text{Fe}]_i \% = m_{\text{HM}} \times w[\text{Fe}]_{\text{HM}} \% + m_{\text{slag}} \times w[\text{FeO}]_{\text{slag}} \% \times 56/72 \quad (1)$$

- Binary basicity:

$$R_2 = \frac{\sum_i m_i \times w(\text{CaO}) \%}{\sum_i m_i \times w(\text{SiO}_2) \%} \quad (2)$$

- Quaternary basicity:

$$R_4 = \frac{\sum_i m_i \times w(\text{CaO}) \% + \sum_i m_i \times w(\text{MgO}) \%}{\sum_i m_i \times w(\text{SiO}_2) \% + \sum_i m_i \times w(\text{Al}_2\text{O}_3) \%} \quad (3)$$

- Quantity of slag:

$$m_{\text{slag}} = \frac{\sum_j m_j}{1 - w(\text{FeO})_{\text{slag}} \%} \quad (4)$$

To enhance the accuracy of the calculation results, the water gas shift reaction in the SRV is taken into account. The volume and composition of syngas generated in the free

space, upper slag zone, and lower slag zone are separately calculated in modules 1–3 by solving four Equations (5)–(8), which include the H element balance, C element balance, equilibrium constant of water gas shift reaction and PCR of the gas.

- H element balance:

$$\sum_i m_i \times w(\text{H})_i \% = 2 \times (V_{\text{H}_2\text{O}} + V_{\text{H}_2}) / 22.4 \quad (5)$$

- C element balance:

$$\sum_i m_i \times w(\text{C})_i \% = m_{\text{HM}} \times w[\text{C}]_{\text{HM}} \% + (V_{\text{CO}} + V_{\text{CO}_2}) \times 12 / 22.4 \quad (6)$$

- PCR:

$$\text{PCR} = (V_{\text{H}_2\text{O}} \% + V_{\text{CO}_2} \% ) / (V_{\text{H}_2\text{O}} \% + V_{\text{CO}_2} \% + V_{\text{H}_2} \% + V_{\text{CO}} \% ) \quad (7)$$

- Equilibrium constant of water gas shift reaction:

$$\begin{aligned} K &= (V_{\text{H}_2} \% \times V_{\text{CO}_2} \% ) / (V_{\text{CO}} \% \times V_{\text{H}_2\text{O}} \% ) \\ &= \text{Exp} [(29490 - 26.8 \times T_{\text{gas}}) / (8.314 \times T_{\text{gas}})] \end{aligned} \quad (8)$$

For the hydrogen-rich process, the volume and composition of syngas generated in each zone are calculated using the same method as shown in Equations (5)–(8). When steam partially replaces  $\text{O}_2$  as the gasifying agent, coal gasification changes from an exothermic reaction to an endothermic reaction [37]. Electric heating is required to provide energy to the furnace. The efficiency of converting electrical energy to thermal energy is reported to be about 70% in the literature [38].

## 2.2. Main Calculation Methods for Uptake Shaft

In addition to the sensible heat of the high-temperature reformed gas, heat is also provided by the  $\text{O}_2$  combustion in the FRS. Consequently, the high-temperature gas discharged from the FRS contains a certain amount of  $\text{CO}_2$  and  $\text{H}_2\text{O}$ . The gas quality can be further improved in the uptake shaft by injecting pulverized coal. The heat and mass balance calculation in the uptake shaft is solved using module 5. The reactions of  $\text{H}_2\text{O}$  with C and  $\text{CO}_2$  with C, as well as the equilibrium of the water gas shift reaction, are taken into account to determine the composition of the reformed gas. The coal consumption is obtained through the iterative calculation of the heat balance.

## 2.3. Main Calculation Methods for FRS

The heat and mass balance in the FRS is calculated with module 6. The off-gas volume and composition are determined by considering the reactions of iron oxide reduction,  $\text{O}_2$  combustion, and the water gas shift reaction. The consumption of  $\text{O}_2$  and recycled gas is iteratively calculated to meet the constraints of the minimum reduction potential and heat balance of the furnace. The definition of reduction potential is shown in Equation (9). The minimum reduction potential of the gas at the outlet is determined with a Baur–Glässner diagram which presents the equilibrium gas composition for iron oxides reduction reactions [27,39,40].

$$R_P = (V_{\text{H}_2} \% + V_{\text{CO}} \% ) / (V_{\text{H}_2\text{O}} \% + V_{\text{CO}_2} \% ) \quad (9)$$

### 3. Results and Discussions

In order to validate the reliability of the present mathematical model, the operational parameters of the HIs melt process were used as inputs, and the results were compared with the plant data [41,42]. The comparison of the calculated slag composition with the actual typical slag composition is presented in Table 1. The results demonstrate a strong agreement between the calculated and actual data. The average relative error is 3.8%.

**Table 1.** Comparison of calculated slag composition with actual slag composition.

Slag Composition	Calculated Data (%)	Actual Data (%)
CaO (Calcium oxide)	35.91	37.47
MgO (Magnesium oxide)	9.30	9.48
SiO <sub>2</sub> (Silicon dioxide)	28.72	30.30
Al <sub>2</sub> O <sub>3</sub> (Aluminium trioxide)	16.48	17.16
FeO (Ferrous oxide)	5.65	5.65

Based on the research experience of existing smelting reduction processes [43–45], it has been noted that the pre-reduction degree of iron ore and the PCR of off-gas are crucial factors that affect the material and energy flows of the process. Therefore, this work also investigates the effect of these two factors. To ensure the quality of syngas, it is assumed that the PCR of SRV off-gas falls within the range of 0–8%. As mentioned in the literature, the reduction rate of iron ore fines is very fast at high temperatures (1473–1673 K), and the final reduction degree is influenced by particle size, reaction time, and gas concentration [24]. For example, when exposed to a 30% H<sub>2</sub> atmosphere, iron ore fines with a particle size of 20–25 µm can reach a reduction degree of approximately 90% within 15 s at 1473 K. Here, considering the complexity of the actual reactor and the use of larger particle sizes of iron ore fines, when discussing the impact of PCR on the inputs and outputs of the process, it is assumed that the average achievable pre-reduction degree of iron ore fines is 70%. Additionally, the impact of the pre-reduction degree of iron ore fines is also discussed within a range of 10–90%, and the PCR is set at 2%. Finally, the effect of H<sub>2</sub> content of the SRV off-gas on the heat and mass balance of the process is examined.

#### 3.1. Effect of PCR of SRV Off-Gas

The combustion reaction between the reducing gas and O<sub>2</sub> takes place in the free space of the SRV, releasing a substantial amount of heat. Figure 4 illustrates the effect of PCR on coal consumption for the production of 1 ton of hot metal in the non-hydrogen-rich process. As the PCR varies from 0% to 8%, the amount of heat transferred from the free space to the upper slag zone also increases, resulting in a significant reduction in coal consumption in this zone from  $5.43 \times 10^3$  kg/tHM to  $1.29 \times 10^3$  kg/tHM. Meanwhile, the coal consumption in the lower slag zone remains relatively low, and only gradually increases within a narrow range of  $0.69 \times 10^3$ – $0.74 \times 10^3$  kg/tHM. The ratio of coal consumption in the upper slag zone to that in the lower slag zone decreases with an increase in PCR, falling within the range of 1.7–7.9 as shown in Figure 4. Additionally, the coal consumption in the uptake shaft also increases within a small range of  $0.52 \times 10^3$ – $0.79 \times 10^3$  kg/tHM. Overall, due to the decrease in coal consumption in the upper slag zone, the total coal consumption decreases by 57% from  $6.55 \times 10^3$  kg/tHM to  $2.82 \times 10^3$  kg/tHM. The total coal consumption under typical operation conditions in the HIs melt process is approximately  $0.9 \times 10^3$  kg/tHM [46], which is only 14–32% of the coal consumption of this technology. In ironmaking processes, it is crucial to minimize coal consumption. However, in this technology, coal serves not only as a reducing agent for iron oxides but also as a raw material for producing synthesis gas. Therefore, high coal consumption is not a concern.

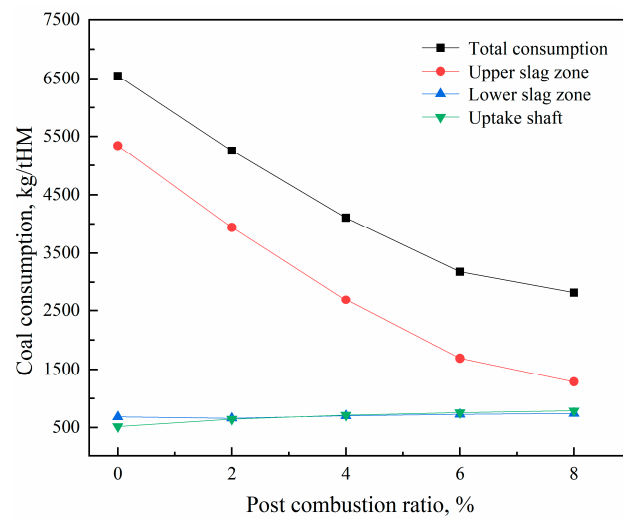


**Figure 4.** Effect of PCR on coal consumption.

The upper limits of  $H_2$  content in the SRV off-gas can be determined under different PCRs, as shown in Figure 5. The calculation is conducted by keeping the total coal consumption of the SRV and conditions the same as those shown in Figure 4, and based on the assumption that all the  $O_2$  injected into the SRV is replaced with steam. The blue lines represent the  $H_2$  and CO contents of SRV off-gas in the non-hydrogen-rich process, while the red lines represent the results in the hydrogen-rich process. For brevity, the non-hydrogen rich process and hydrogen-rich process are, respectively, referred to as process 1 and process 2 in the following figures. As the PCR increases from 0% to 8%, there is a corresponding decrease in the upper limit of  $H_2$  content from 52.7% to 45.2%, and there is a linear inverse relationship between the two. The relationship between the PCR and the upper limit of  $H_2$  content can be obtained as shown in Figure 5. In process 1, the  $H_2$  content ranges from 19.6% to 16.6%. Therefore, the operation window for  $H_2$  enrichment in the SRV is obtained and shown between the red circular dotted line and the blue circular dotted line in the figure. In process 1, CO is the main component. In process 2, however, the  $H_2$  content is slightly higher than the CO content. Additionally, the evidence shows that the higher the PCR, the lower the  $H_2$  content in the syngas produced from SRV. The  $H_2$  contents in the syngas of Lurgi and British Gas Lurgi coal gasification processes are approximately 40% and 25% [8], respectively. It can be seen that this process has significant improvements in hydrogen enrichment.

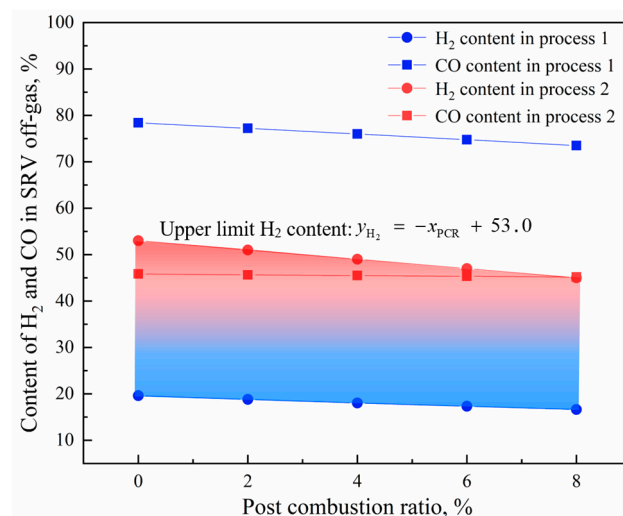


**Figure 5.** Effect of PCR on upper limit of  $H_2$  content.

As previously mentioned, a portion of the reformed gas is recycled to the FRS as reducing gas and fuel, and the remaining reformed gas is output as a product. The effect of PCR on the off-gas volume of the FRS and SRV, as well as on the volume of recycled gas and exported gas under process 1 and 2, is analyzed and illustrated in Figure 6. To study the effect of PCR under the same conditions, in the cases of process 2, the H<sub>2</sub> content in the SRV off-gas is set at 45%, which is close to the upper limit of H<sub>2</sub> content when the PCR is 8%. It can be seen that the volume of SRV off-gas under both processes decreases with the increase in PCR, while the volume of FRS off-gas increases, as shown in Figure 6a. The SRV off-gas volume under process 2 is approximately 1.5 times as much as that under process 1. Consequently, the total reformed gas volume under process 2 is also higher than that under process 1, as shown in Figure 6b. On the other hand, since the H<sub>2</sub> content of the reformed gas in process 2 is higher than that in process 1, the amount of recycled gas needed by the FRS is reduced. It can be observed that as PCR increases from 0 to 8%, the proportion of the exported gas volume to the total reformed gas volume decreases from 80% to 63% in process 1 and from 88% to 77% in process 2. Overall, the exported gas volume in process 2 is approximately 1.4 times as much as that in process 1 at the same PCR. Additionally, as the PCR varies from 0% to 8%, the exported gas volume in process 1 decreases by 53% from  $1.25 \times 10^4 \text{ Nm}^3/\text{tHM}$  to  $0.58 \times 10^4 \text{ Nm}^3/\text{tHM}$ , and the exported gas volume in process 2 decreases by 50% from  $1.79 \times 10^4 \text{ Nm}^3/\text{tHM}$  to  $0.88 \times 10^4 \text{ Nm}^3/\text{tHM}$ . According to the literature [35], the exported gas volume in the HIs melt process is approximately  $3.6 \times 10^3 \text{ Nm}^3/\text{tHM}$  and the PCR of the gas is approximately 50–60%. Compared to the HIs melt process, this technology produces a larger amount of gas per ton of hot metal and can also yield a higher quality gas product.

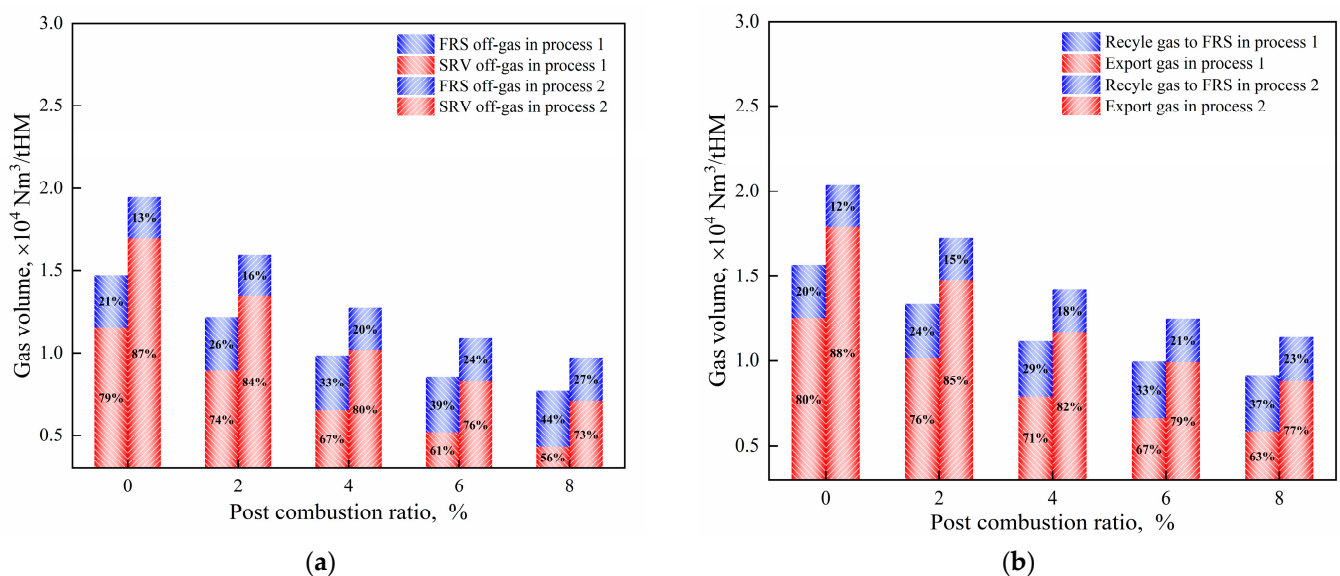


**Figure 6.** Effect of PCR on gas volume: (a) volume of FRS off-gas and SRV off-gas (b) volume of recycled gas and exported gas.

The CO and H<sub>2</sub> contents in the mixture of SRV off-gas and FRS off-gas (before reforming), as well as in the exported gas (after reforming), are depicted in Figure 7 for the cases presented in Figure 6. The solid lines represent the contents of the gas mixture before reforming, while the dashed lines represent the contents of the gas after reforming. As seen in Figure 7, the CO and H<sub>2</sub> contents before reforming decrease as PCR increases. However, in process 1, the CO and H<sub>2</sub> contents after reforming can reach approximately 78% and 20%, while in process 2, they can reach approximately 54% and 44%, respectively. The reduction potential of the reformed gas is close to one when the PCR is below 8%. The H<sub>2</sub> content in the syngas after reforming is quite close to that (45%) in the SRV off-gas, and the difference can be ignored.

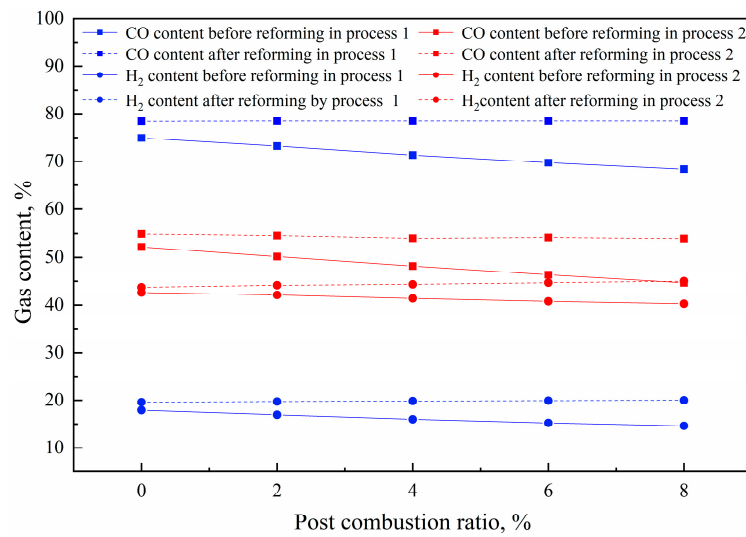


Figure 7. Gas contents before and after reforming.

In the SRV, the ratio of O<sub>2</sub> consumption in the upper slag zone to that in the lower slag zone is generally consistent with the ratio of coal consumption. Therefore, the O<sub>2</sub> consumption in the entire molten slag, as well as in the free space of the SRV and in the FRS, is calculated under different PCRs, as shown in Figure 8. The calculation conditions are the same as those in Figure 6. It can be clearly seen that the total O<sub>2</sub> consumption in the SRV of process 1 is greater than that of process 2, as O<sub>2</sub> is partially replaced with steam in the latter. As the PCR varies from 0% to 8%, the O<sub>2</sub> consumption in the free space of both processes slowly increases. Moreover, process 2 requires a greater amount of O<sub>2</sub> in the free space compared to process 1 at the same PCR. The main reason is that more syngas is produced in the molten slag through steam injection. The O<sub>2</sub> consumption in the molten slag of process 1 decreases significantly by 65%. In the FRS, the O<sub>2</sub> consumption of both processes slightly increases with the increase in PCR, as the temperature of the recycled gas decreases with the increase in PCR. Due to the lower combustion heat of H<sub>2</sub> compared to CO, the O<sub>2</sub> consumption in the FRS of process 2, as shown in Figure 8, is slightly higher than that of process 1 under the same conditions. The total O<sub>2</sub> consumption in process 1 decreases by 57% from  $4.28 \times 10^3 \text{ Nm}^3/\text{tHM}$  to  $1.82 \times 10^3 \text{ Nm}^3/\text{tHM}$  and decreases by 67% from  $1.58 \times 10^3 \text{ Nm}^3/\text{tHM}$  to  $0.53 \times 10^3 \text{ Nm}^3/\text{tHM}$  in process 2.

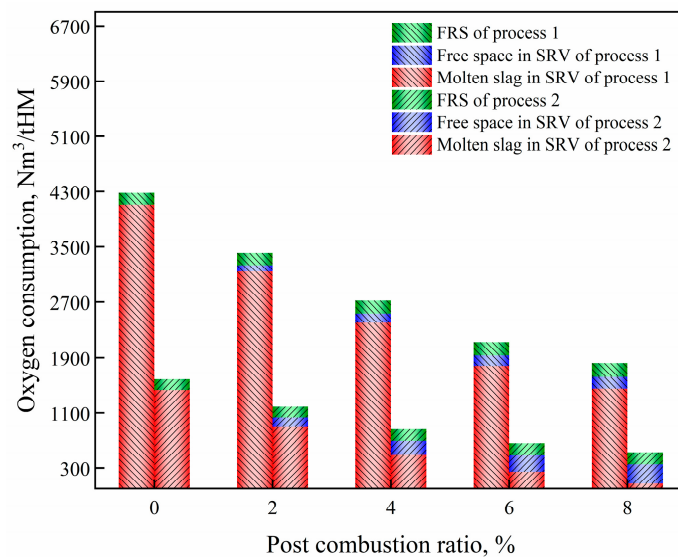
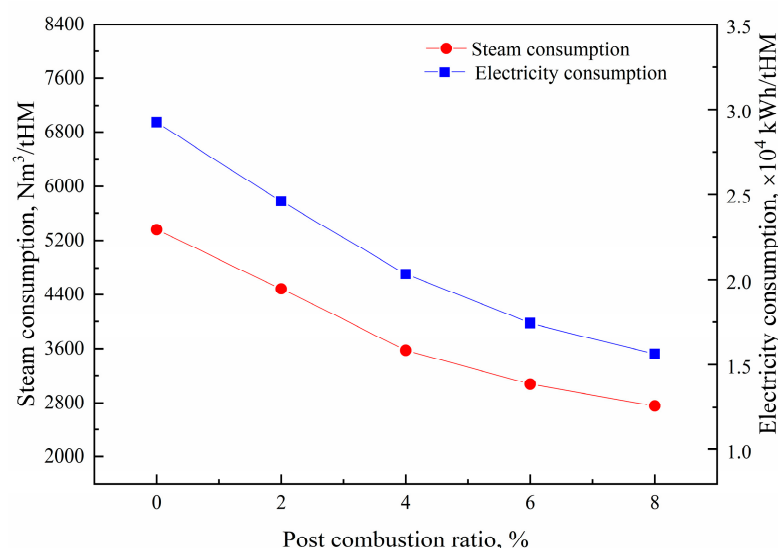


Figure 8. Oxygen consumption in both processes at different PCRs.

The difference in O<sub>2</sub> consumption in the molten slag between the two processes at the same PCR, as shown in Figure 8, requires twice the volume of steam to maintain the same coal consumption. The effect of PCR on the steam consumption and the electricity consumption in process 2 is given in Figure 9. Both steam and electricity consumption decrease with an increase in PCR. At the current conditions, the steam consumption ranges from  $5.34 \times 10^3 \text{ Nm}^3/\text{tHM}$  to  $2.76 \times 10^3 \text{ Nm}^3/\text{tHM}$ , and the electricity consumption ranges from  $2.92 \times 10^4 \text{ kWh/tHM}$  to  $1.56 \times 10^4 \text{ kWh/tHM}$ . Both of these values are reduced by approximately 48% as the PCR increases from 0% to 8%.



**Figure 9.** Effect of PCR on steam and electricity consumption in the hydrogen-rich process.

### 3.2. Effect of Pre-Reduction Degree of Iron Ore

Figure 10 illustrates the effect of the pre-reduction degree of iron ore fines on the coal consumption in process 1. The pre-reduction degree ranges from 10% to 90%. As the pre-reduction degree increases, less coal is needed in the upper slag zone as a fuel for heating the materials, and less coal is needed as a reducing agent in the lower slag zone for iron oxides reduction. At the current conditions, the ratio of coal consumption in the upper slag zone to that in the lower slag zone increases in the range of 3.6–5.7 as the pre-reduction degree increases. Additionally, the coal consumption in the uptake shaft increases linearly with the increase in the pre-reduction degree. This is because a higher reduction degree in the FRS requires a larger amount of reducing gas, which in turn necessitates a greater amount of coal for gas reforming in the uptake shaft. Ultimately, the total coal consumption decreases by 47% from  $8.12 \times 10^3 \text{ kg/tHM}$  to  $4.27 \times 10^3 \text{ kg/tHM}$  as the pre-reduction degree increases from 10% to 90%.

Under the same conditions as those in Figure 10, the upper limits of H<sub>2</sub> content in the SRV off-gas have been obtained under different pre-reduction degrees, as shown in Figure 11. Unlike the influence of PCR, the pre-reduction degree has little effect on the upper limit of H<sub>2</sub> content (red circular dotted line) which maintains at approximately 50–51%. This value is about 5% higher than the CO content produced by process 2 and approximately 32% higher than the H<sub>2</sub> content produced by process 1. The operation window for H<sub>2</sub> enrichment is the area between the red circular dotted line and the blue circular dotted line in Figure 11.

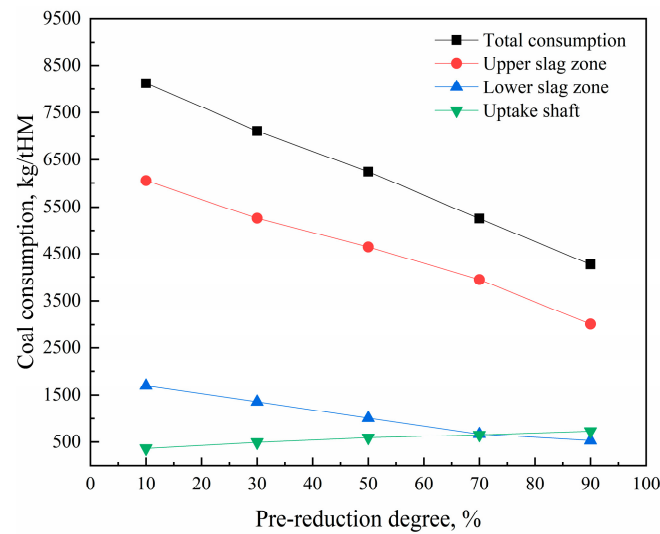


Figure 10. Effect of pre-reduction degree on coal consumption.

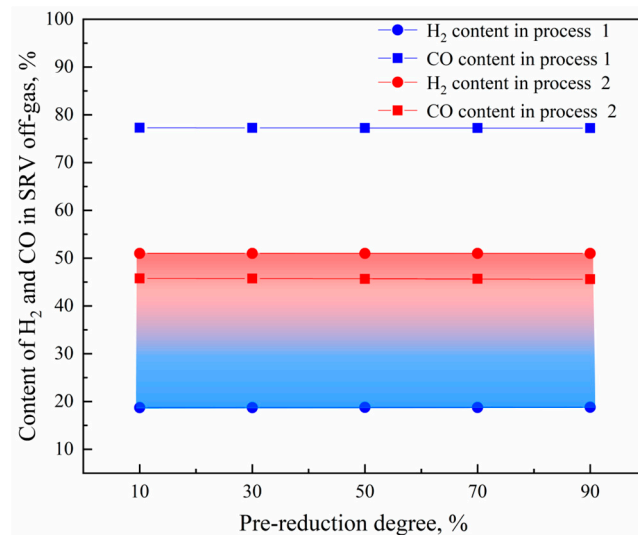
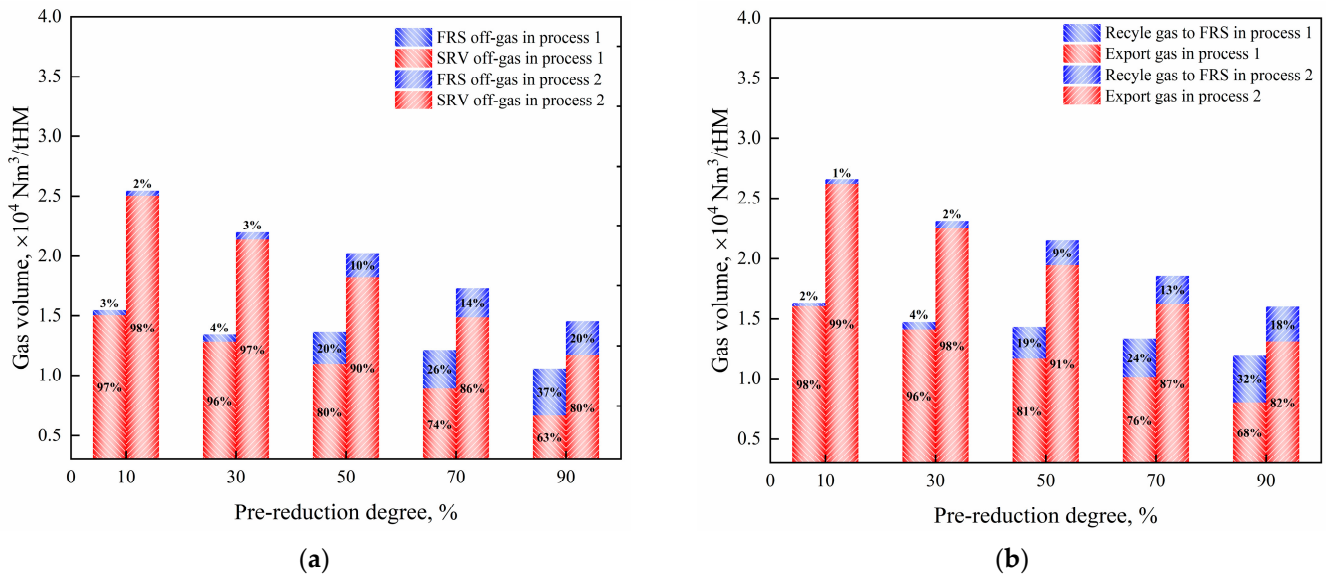


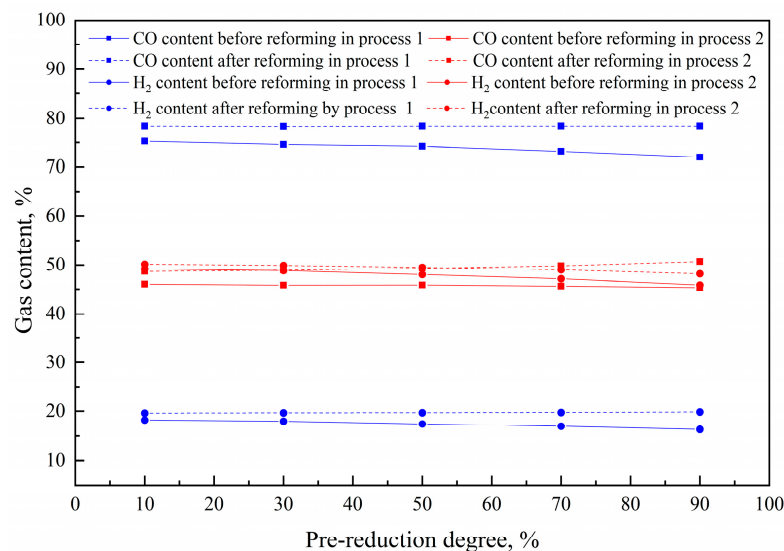
Figure 11. Effect of pre-reduction degree on upper limit of H<sub>2</sub> content.

Figure 12 shows the effect of the pre-reduction degree on the off-gas volume of the FRS and SRV, as well as on the volume of recycled gas and exported gas under the two processes. In the cases of process 2, the H<sub>2</sub> content in SRV off-gas is set at 50%, which is close to the upper limit of H<sub>2</sub> content when the PCR is 2%. The volume of SRV off-gas decreases while the volume of FRS off-gas increases with the increase in the pre-reduction degree, as shown in Figure 12a. The main reason for this is that the amount of reducing gas required by the FRS (recycled gas) increases with the increase in the pre-reduction degree, and the coal consumption in the SRV decreases accordingly (as shown in Figure 10). The SRV off-gas volume under process 2 is approximately 1.7 times as much as that under process 1. Due to the higher H<sub>2</sub> content of the reformed gas in process 2, the recycled gas needed by the FRS is reduced compared to process 1. This is particularly evident in the cases of high pre-reduction degree as shown in Figure 12b. It can be seen that the proportion of the exported gas volume to the total reformed gas volume decreases from 98% to 68% in process 1 and from 99% to 82% in process 2. On the other hand, the exported gas volume in process 2 is approximately 1.6 times as much as that in process 1 at the same pre-reduction degree. Furthermore, as the pre-reduction degree varies from 10% to 90%, the volume of exported gas decreases by 50% in both processes.



**Figure 12.** Effect of pre-reduction degree on gas volume: (a) volume of FRS off-gas and SRV off-gas, (b) volume of recycled gas and exported gas.

The CO and H<sub>2</sub> contents in the gas before and after reforming are further given in Figure 13. In both processes, the CO and H<sub>2</sub> contents are increased by reforming, resulting in a final reduction potential close to one. In process 1, the CO and H<sub>2</sub> contents after reforming can reach approximately 78% and 20%, respectively. In process 2, the H<sub>2</sub> content is slightly higher than the CO content in the gas before reforming when the pre-reduction degree is between 10 and 90%. After reforming, when the pre-reduction degree is lower than 50%, the H<sub>2</sub> content is still slightly higher than the CO content. However, when the pre-reduction degree is higher than 50%, the opposite is true. In general, the content of both gases after reforming in process 2 is around 50%, which is close to the gas content in the SRV off-gas.



**Figure 13.** Gas content before and after reforming.

The O<sub>2</sub> consumption in the molten slag and free space of SRV, as well as in the FRS under different pre-reduction degrees, is illustrated in Figure 14. In the case of process 2, a portion of the O<sub>2</sub> in the SRV is replaced with steam to achieve a high H<sub>2</sub> content. Therefore, the O<sub>2</sub> consumption of process 2 is significantly lower than that of process 1. Additionally,

in process 1, the  $O_2$  consumption in the molten slag decreases by 55% as the pre-reduction degree varies from 10% to 90%, aligning with the variation of coal consumption in the SRV. Since the gas volume generated in the molten slag decreases with the increase in the pre-reduction degree, the amount of  $O_2$  used for combustion in the free space decreases accordingly. For both processes, the  $O_2$  consumption in the FRS also increases with the increase in the pre-reduction degree, as a larger amount of recycled gas is required to achieve a higher pre-reduction degree (as shown in Figure 12).

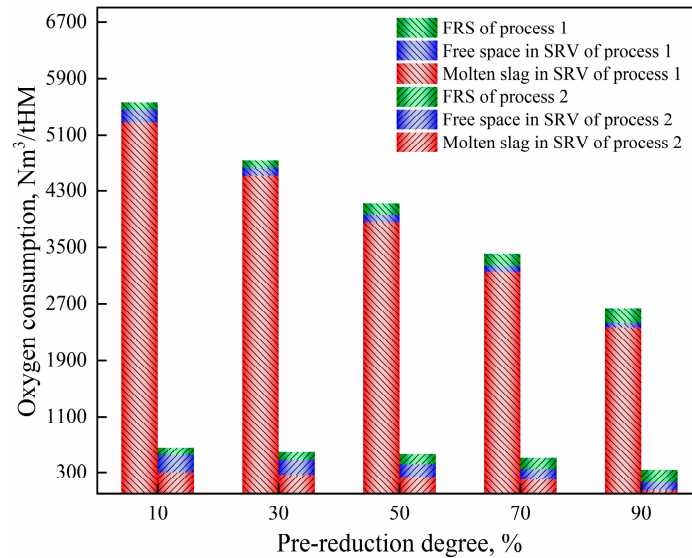


**Figure 14.** Oxygen consumption in both processes at different pre-reduction degrees.

The effect of the pre-reduction degree on steam consumption and electricity consumption in process 2 is shown in Figure 15. Both steam consumption and the electricity consumption decrease linearly with the increase in the pre-reduction degree. At the current conditions, the steam consumption ranges from  $9.95 \times 10^3 \text{ Nm}^3/\text{tHM}$  to  $4.64 \times 10^3 \text{ Nm}^3/\text{tHM}$ , and the electricity consumption ranges from  $5.78 \times 10^4 \text{ kWh/tHM}$  to  $2.67 \times 10^4 \text{ kWh/tHM}$ . Both of these values reduce by approximately 53% as the pre-reduction degree increases from 10% to 90%.

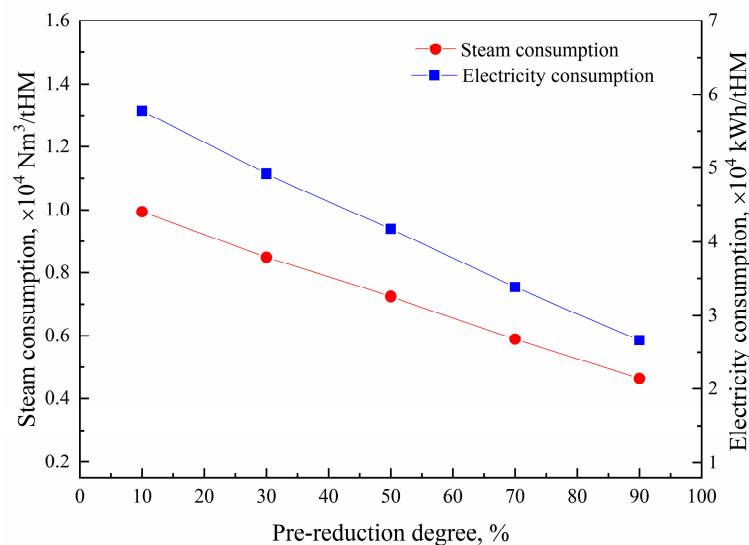


**Figure 15.** Effect of pre-reduction degree on steam and electricity consumption in the hydrogen-rich process.

### 3.3. Effect of H<sub>2</sub> Content of the SRV Off-Gas

Figure 16 gives the effect of H<sub>2</sub> content in the SRV off-gas on the off-gas volume of the FRS and SRV, as well as on the volume of recycled gas and exported gas in the two processes. The pre-reduction degree of iron ore and the PCR of SRV off-gas are set at 70% and 2%, respectively. When the H<sub>2</sub> content varies from 30% to 50%, the off-gas volume of SRV increases from  $1.05 \times 10^4 \text{ Nm}^3/\text{tHM}$  to  $1.46 \times 10^4 \text{ Nm}^3/\text{tHM}$  due to more carbon reacting with steam in the reactor. Despite the off-gas volume of FRS decreasing gradually, the total off-gas volume (SRV + FRS) still exhibits an upward trend with the increase in H<sub>2</sub> content. Consequently, the total gas volume after reforming gradually increases. On the other hand, an increase in H<sub>2</sub> content reduces the recycled gas volume, which leads to a larger exported gas volume under high H<sub>2</sub> content compared to low H<sub>2</sub> content. It can be observed that the proportion of the exported gas volume compared to the total reformed gas volume is not lower than 71% under the current conditions. Furthermore, as the H<sub>2</sub> content increases from 30% to 50%, the exported gas volume experiences a significant 38% increase.

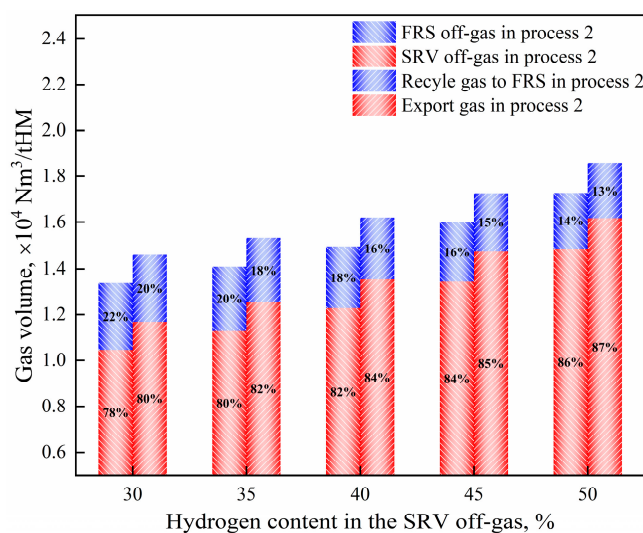


Figure 16. Effect of H<sub>2</sub> content on gas volume at the inlet and outlet of zones.

Figure 17 shows the effect of H<sub>2</sub> content in the SRV off-gas on the consumption of steam, O<sub>2</sub>, and electricity for the production of 1 ton of hot metal. As the H<sub>2</sub> content increases from 30% to 50%, the consumption of steam and electricity increases dramatically by approximately three times, while the O<sub>2</sub> consumption decreases accordingly. The primary reason is that the increase in the desired H<sub>2</sub> content must be achieved by increasing the amount of steam injection. At the same time, the oxygen provided by the steam also increases, resulting in a decrease in the demand for additional O<sub>2</sub>. Due to the increase in heat absorption from the reaction between steam and coal, electricity consumption also increases. When the H<sub>2</sub> content reaches 50%, which closely resembles the composition of water gas, the steam consumption is approximately  $5.89 \times 10^3 \text{ Nm}^3/\text{tHM}$ .

Figure 18 illustrates the effect of H<sub>2</sub> content on the reformed gas temperature under different PCRs. When the PCR is higher than 2%, the H<sub>2</sub> content cannot reach 50%. It can be observed that the temperature of reformed gas increases with the increase in H<sub>2</sub> content in the SRV off-gas, while it decreases with the increase in PCR. The main reason is that the increase in PCR can increase the content of CO<sub>2</sub> and H<sub>2</sub>O in the gas before reforming. However, increasing the H<sub>2</sub> content can reduce the CO<sub>2</sub> and H<sub>2</sub>O contents in the gas before reforming. As there is a linear relationship between the reformed gas temperature and the H<sub>2</sub> content, the reformed gas temperature can be calculated by the fitted functions as shown in Figure 18. According to the calculation results, the temperature of gas before reforming under the current conditions is around 1412 °C. Therefore, the temperature drop

in the uptake shaft is in the range of 77–229 °C. Compared to the HIs melt process (off-gas temperature: 1450 °C), the more sensible heat of syngas is utilized to improve gas quality.

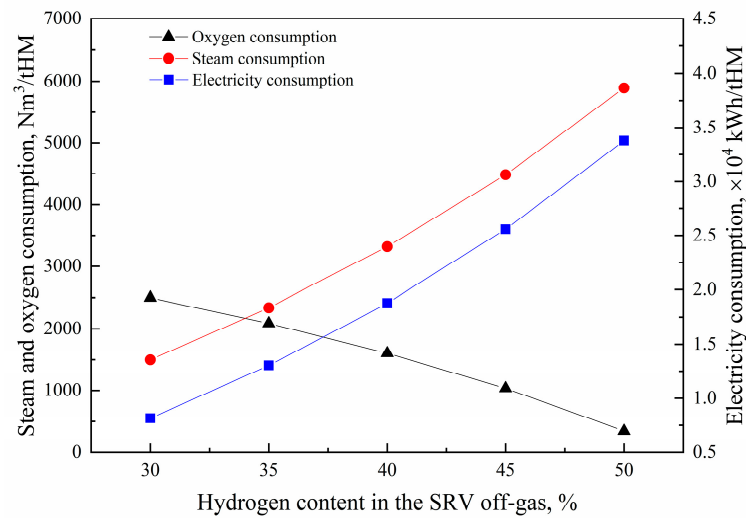


Figure 17. Effect of H<sub>2</sub> content on consumption of steam, O<sub>2</sub> and electricity.

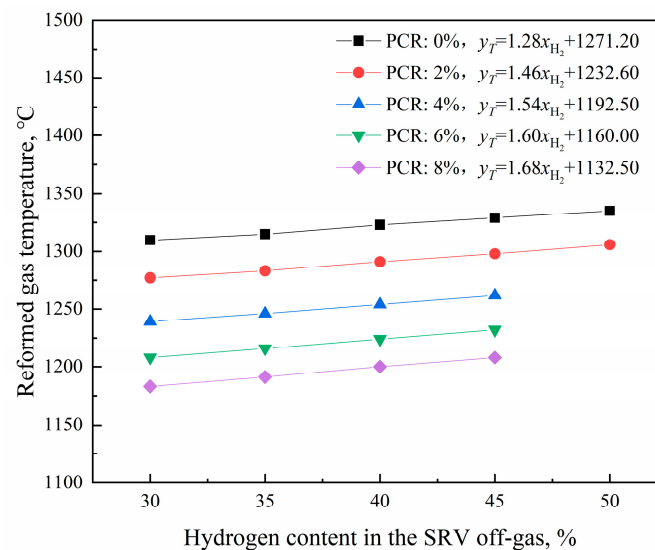


Figure 18. Effect of H<sub>2</sub> content on reformed gas temperature under different PCRs.

#### 4. Conclusions

A multi-zone constrained mathematical model has been developed to predict the performance of an integrated technology for smelting reduction ironmaking and coal gasification. The calculation results can provide a theoretical basis for the development and optimization of this integrated technology. Additionally, the model can be utilized to provide operators with better control over process parameters.

The results reveal that this technology can successfully couple the manufacturing of iron and syngas. The H<sub>2</sub> content in the syngas can be greatly increased by injecting steam into the SRV. Under the current studied conditions, the increase in the PCR of SRV off-gas and the pre-reduction degree of iron ore fines can significantly reduce the total coal consumption and the exported gas volume for producing 1 ton of hot metal. The upper limit of H<sub>2</sub> content in the SRV off-gas is primarily determined by the PCR, while the pre-reduction degree has little effect on it. For this new and complicated technology, further exploration is required to understand the many reaction kinetics, transport phenomena and energy consumption involved in the furnace. Furthermore, it is important to assess

the effect of varying electricity prices and coal costs on the overall cost for producing hot metal and syngas. This will provide a more comprehensive understanding of the economic viability of the integrated technology and help to identify any potential areas for optimization.

**Author Contributions:** Conceptualization, Y.Q. and S.S.; methodology, Y.Q., Z.Z., S.S. and L.S.; validation, Y.Q. and L.S.; formal analysis, Y.Q. and S.S.; writing original draft preparation, Y.Q.; supervision L.S. and Z.Z.; project administration, Y.Q., Z.Z. and L.S.; funding acquisition, L.S. All authors have read and agreed to the published version of the manuscript.

**Funding:** This research was funded by the National Natural Science Foundation of China, grant number 52374329.

**Data Availability Statement:** Data are contained within the article.

**Conflicts of Interest:** The authors declare no conflicts of interest.

## Abbreviations

$m$	mass, kg
$w[\text{Fe}]%$	weight percentage of Fe
$w(\text{FeO})%$	weight percentage of FeO
$R_2$	binary basicity
$R_4$	quaternary basicity
$w(\text{CaO})%$	weight percentage of CaO in slag
$w(\text{SiO}_2)%$	weight percentage of SiO <sub>2</sub> in slag
$w(\text{MgO})%$	weight percentage of MgO in slag
$w(\text{Al}_2\text{O}_3)%$	weight percentage of Al <sub>2</sub> O <sub>3</sub> in slag
$w(\text{H})%$	weight percentage of hydrogen
$w(\text{C})%$	weight percentage of carbon
$V_{\text{H}_2\text{O}}$	volume of H <sub>2</sub> O, Nm <sup>3</sup>
$V_{\text{H}_2}$	volume of H <sub>2</sub> , Nm <sup>3</sup>
$V_{\text{CO}}$	volume of CO, Nm <sup>3</sup>
$V_{\text{CO}_2}$	volume of CO <sub>2</sub> , Nm <sup>3c</sup>
$PCR$	post combustion ratio, %
$T_{\text{off-gas}}$	off-gas temperature, °C
$K$	equilibrium constant of water gas shift reaction
$V_{\text{H}_2}%$	volume percentage of H <sub>2</sub> , %
$V_{\text{CO}}%$	volume percentage of CO, %
$V_{\text{H}_2\text{O}}%$	volume percentage of H <sub>2</sub> O, %
$V_{\text{CO}_2}%$	volume percentage of CO <sub>2</sub> , %
$R_p$	reduction potential
$i$	a type of raw material
$j$	a component in slag
HM	hot metal
Slag	related to the slag

## References

- Finkelman, R.B.; Wolfe, A.; Hendryx, M.S. The future environmental and health impacts of coal. *Energy Geosci.* **2021**, *2*, 99–112. [[CrossRef](#)]
- Zhou, H.; Bhattarai, R.; Li, Y.; Si, B.; Dong, X.; Wang, T.; Yao, Z. Towards sustainable coal industry: Turning coal bottom ash into wealth. *Sci. Total Environ.* **2022**, *804*, 149985. [[CrossRef](#)]
- Sun, J.; Luo, K.; Feng, H.; Fan, C.; Jin, H.; Guo, L. Experimental investigation on organic functional groups evolution in hydrogen production process by coal gasification in supercritical water. *Int. J. Hydrogen Energy* **2023**, *48*, 5887–5900. [[CrossRef](#)]
- Yin, Z.; Xu, H.; Chen, Y.; Zhao, T.; Wu, J. Experimental simulate on hydrogen production of different coals in underground coal gasification. *Int. J. Hydrogen Energy* **2023**, *48*, 6975–6985. [[CrossRef](#)]
- Dai, F.; Zhang, S.; Luo, Y.; Wang, K.; Liu, Y.; Ji, Y. Recent progress on hydrogen-rich syngas production from coal gasification. *Processes* **2023**, *11*, 1765. [[CrossRef](#)]
- Stenina, I.; Yaroslavtsev, A. Modern technologies of hydrogen production. *Processes* **2022**, *11*, 56. [[CrossRef](#)]

7. Chyou, Y.P.; Chiu, H.M.; Chen, P.C.; Chien, H.Y.; Wang, T. Coal-derived synthetic natural gas as an alternative energy carrier for application to produce power—Comparison of integrated vs. non-integrated processes. *Energy* **2023**, *282*, 128958. [[CrossRef](#)]
8. Qin, S.; Zhang, X.; Wang, M.; Cui, H.; Li, Z.; Yi, W. Comparison of BGL and Lurgi gasification for coal to liquid fuels (CTL): Process modeling, simulation and thermodynamic analysis. *Energy* **2021**, *229*, 120697. [[CrossRef](#)]
9. Gu, J.; Yang, S.; Kokossis, A. Modeling and analysis of coal-based Lurgi gasification for LNG and methanol coproduction process. *Processes* **2019**, *7*, 688. [[CrossRef](#)]
10. Nakajima, H.; Anezaki, S.; Tozaki, Y.; Ichihara, K.; Katohgi, K. Improvement of the heat balance in the combined blowing process. *Trans. Iron Steel Inst. Jpn.* **1986**, *26*, 40–47. [[CrossRef](#)]
11. Okamura, S.; Sueyasu, M.; Fukuda, M.; Furujo, S.; Okane, K. Coal gasification using a molten iron bath. *Fuel* **1982**, *61*, 1027–1031. [[CrossRef](#)]
12. Barin, I.; Modigell, M.; Sauert, F. Thermodynamics and kinetics of coal gasification in a liquid iron bath. *Metall. Trans. B* **1987**, *18*, 347–354. [[CrossRef](#)]
13. Eatwell-Hall, R.E.A.; Sharifi, V.N.; Swithenbank, J. Hydrogen production from molten metal gasification. *Int. J. Hydrogen Energy* **2010**, *35*, 13168–13178. [[CrossRef](#)]
14. Yohan, R.; Joel, B.; Anne, J. A short overview on purification and conditioning of syngas produced by biomass gasification: Catalytic strategies, process intensification and new concepts. *Prog. Energy Combust.* **2012**, *38*, 765–781.
15. Cao, C.; Meng, Y.; Yan, F.; Zhang, D.; Li, X.; Zhang, F. Analysis on energy efficiency and optimization of HIs melt process. In *Energy Technology 2019*; CpG Islands; Springer: Berlin/Heidelberg, Germany, 2019.
16. Khasraw, D.; Spooner, S.; Hage, H.; Meijer, K.; Li, Z. Evaluation of devolatilization behaviour of different carbonaceous materials under rapid heating for the novel HIsarna ironmaking process. *Fuel* **2021**, *292*, 120329. [[CrossRef](#)]
17. Sohn, H.Y.; Fan, D.Q.; Abdelghany, A. Design of novel flash ironmaking reactors for greatly reduced energy consumption and CO<sub>2</sub> emissions. *Metals* **2021**, *11*, 332. [[CrossRef](#)]
18. Hosseini, A.; Hage, J.L.T.; Duiker, A.; Meijer, L.; Peeters, T.; Offerman, E.; Yang, Y. Off-Gas system scale-up of HIsarna iron-making process: A cfd-based approach. *Metall. Mater. Trans. B* **2022**, *53*, 3557–3574. [[CrossRef](#)]
19. Htet, T.T.; Yan, Z.; Spooner, S.; Degirmenci, V.; Meijer, K. Gasification and physical-chemical characteristics of carbonaceous materials in relation to HIsarna ironmaking process. *Fuel* **2021**, *289*, 119890. [[CrossRef](#)]
20. Hosseini, A.; Dhiman, V.; Meijer, K.; Zeilstra, C.; Hage, J.; Peeters, T.; Offerman, E.; Yang, Y. CFD modelling of the off-gas system of HIsarna iron making process. Part 1: Model development using detailed reaction mechanism for post-combustion of CO–H<sub>2</sub> mixture and carbon particles. *Ironmak. Steelmak.* **2022**, *49*, 828–844. [[CrossRef](#)]
21. Fan, D.Q.; Elzohiery, M.; Mohassab, Y.; Sohn, H.Y. The kinetics of carbon monoxide reduction of magnetite concentrate particles through cfd modelling. *Ironmak. Steelmak.* **2021**, *48*, 769–778. [[CrossRef](#)]
22. Elzohiery, M.; Fan, D.; Mohassab, Y.; Sohn, H.Y. Kinetics of hydrogen reduction of magnetite concentrate particles at 1623–1873 K relevant to flash ironmaking. *Ironmak. Steelmak.* **2021**, *48*, 485–492. [[CrossRef](#)]
23. Fan, D.; Elzohiery, M.; Mohassab, Y.; Sohn, H.Y. Rate-enhancement effect of CO in magnetite concentrate particle reduction by H<sub>2</sub> + CO mixtures. *Ironmak. Steelmak.* **2021**, *48*, 1064–1075. [[CrossRef](#)]
24. Wang, H.; Sohn, H.Y. Hydrogen reduction kinetics of magnetite concentrate particles relevant to a novel flash ironmaking process. *Metall. Mater. Trans. B* **2013**, *44*, 133–145. [[CrossRef](#)]
25. Yan, Z.; Htet, T.T.; Hage, J.; Meijer, K.; Li, Z. HIsarna process simulation model: Using factsage with macro facility. *Metall. Mater. Trans. B* **2023**, *54*, 868–879. [[CrossRef](#)]
26. Wang, Z.; Li, R.; Zong, Y.; Hu, P.; Zhang, J. Simulation of the flow, temperature, and concentration fields in the reactor of the HIs melt process. *Ironmak. Steelmak.* **2022**, *49*, 968–975. [[CrossRef](#)]
27. He, Y.; Tang, B.; Li, Q.; Zou, Z. A comprehensive static model of an iron bath smelting reduction process with thick slag for alumina-rich iron ore. *ISIJ Int.* **2015**, *55*, 2125–2134. [[CrossRef](#)]
28. Ariyama, T.; Takahashi, K.; Kawashiri, Y.; Nouchi, T. Diversification of the ironmaking process toward the long-term global goal for carbon dioxide mitigation. *J. Sustain. Metall.* **2019**, *5*, 276–294. [[CrossRef](#)]
29. Vidhyasagar, M.; Kumar, D.; Viswanathan, N.N.; Kumar, S.M.; Manjini, A. A static model for energy-optimizing furnace. *Steel Res. Int.* **2022**, *93*, 2200185. [[CrossRef](#)]
30. Wang, H.; Yu, H.; Teng, L.; Seetharaman, S. Evaluation on material and heat balance of EAF processes with introduction of CO<sub>2</sub>. *J. Min. Metall. B.* **2016**, *52*, 1–8. [[CrossRef](#)]
31. Bhaskar, A.; Assadi, M.; Somehsaraei, H.N. Decarbonization of the iron and steel industry with direct reduction of iron ore with green hydrogen. *Energies* **2020**, *13*, 758. [[CrossRef](#)]
32. Jampani, M.; Gibson, J.; Pistorius, P.C. Increased use of natural gas in blast furnace ironmaking: Mass and energy balance calculations. *Metall. Mater. Trans. B* **2019**, *50*, 1290–1299. [[CrossRef](#)]
33. Kou, M.; Zhou, H.; Wu, S.; Shen, T. Static model study on the characteristics of coke oven gas dome injection in COREX melter gasifier. *Arch. Metall. Mater.* **2020**, *65*, 275–281. [[CrossRef](#)]
34. Yang, Y.; Guo, L.; Li, D.; Guo, Z. Numerical analysis of gasification characteristics in combined coal gasification and flash ironmaking process. *Appl. Therm. Eng.* **2020**, *171*, 115067. [[CrossRef](#)]
35. Pang, Z.; Bu, J.; Yuan, Y.; Zheng, J.; Xue, Q.; Wang, J.; Guo, H.; Zuo, H. The low-carbon production of iron and steel industry transition process in China. *Steel Res. Int.* **2023**, 2300500. [[CrossRef](#)]

36. Chen, W.H.; Lin, B.J. Hydrogen and synthesis gas production from activated carbon and steam via reusing carbon dioxide. *Appl. Energy* **2013**, *101*, 551–559. [[CrossRef](#)]
37. Sadasivam, S.; Zagorščak, R.; Thomas, H.R.; Kapusta, K.; Stańczyk, K. Experimental study of methane-oriented gasification of semi-anthracite and bituminous coals using oxygen and steam in the context of underground coal gasification (UCG): Effects of pressure, temperature, gasification reactant supply rates and coal rank. *Fuel* **2020**, *268*, 117330. [[CrossRef](#)]
38. Logar, V.; Dovžan, D.; Škrjanc, I. Modeling and validation of an electric arc furnace: Part 1, heat and mass transfer. *ISIJ Int.* **2012**, *52*, 402–412. [[CrossRef](#)]
39. Kim, T.; Yoon, S.; Lee, S.; Sohn, I. Investigation of (H<sub>2</sub>–H<sub>2</sub>O) partial pressure on the gas-based reduction of fine iron ore in mixed gases (H<sub>2</sub>–H<sub>2</sub>O–CO–CO<sub>2</sub>–N<sub>2</sub>). *J. Mater. Res. Technol.* **2024**, *29*, 323–334. [[CrossRef](#)]
40. Marques-Valderrama, I.; Becerra, J.A.; Ortiz, C.; Rodríguez-Pastor, D.A.; Chacartegui, R. Efficiency, cost, optimization, simulation and environmental impact of energy systems. In Proceedings of the 36th International Conference on Efficiency Analysis in the Chemical Loop Process of Base Metals, Las Palmas de Gran Canaria, Spain, 25 June 2023.
41. Feng, J.; Wang, Z.; Zhang, J.; Zhang, S. Construction and verification of energy and mass transfer model of Hlsmelt smelting reduction main reactor. *Iron Steel* **2022**, *57*, 57–64.
42. Zhang, J.; Li, K.; Zhang, G.; Wang, Z.; Zhang, X. Technological innovation and latest production index of shandong molong Hlsmelt process. *Ironmak* **2018**, *37*, 56–60.
43. Srishilan, C.; Shukla, A.K. Thermodynamic model of COREX melter gasifier using factSage™ and macro facility. *Metall. Mater. Trans. B* **2019**, *50*, 312–323. [[CrossRef](#)]
44. Qu, Y.; Zou, Z.; Xiao, Y. A comprehensive static model for COREX process. *ISIJ Int.* **2012**, *52*, 2186–2193. [[CrossRef](#)]
45. Srishilan, C.; Shukla, A.K. Static thermochemical model of COREX melter gasifier. *Metall. Mater. Trans. B* **2018**, *49*, 388–398. [[CrossRef](#)]
46. Liu, W.; Zuo, H.; Wang, J.; Xue, Q.; Ren, B.; Yang, F. The production and application of hydrogen in steel industry. *Int. J. Hydrogen Energy* **2021**, *46*, 10548–10569. [[CrossRef](#)]

**Disclaimer/Publisher’s Note:** The statements, opinions and data contained in all publications are solely those of the individual author(s) and contributor(s) and not of MDPI and/or the editor(s). MDPI and/or the editor(s) disclaim responsibility for any injury to people or property resulting from any ideas, methods, instructions or products referred to in the content.